



Electrospinning ZnO/carbon nanofiber as binder-free and self-supported anode for Li-ion batteries



Hui Ning¹, Hui Xie¹, Qingshan Zhao, Jialiang Liu, Wei Tian, Yixian Wang, Mingbo Wu*

State Key Laboratory of Heavy Oil Processing, College of Chemical Engineering, China University of Petroleum, Qingdao 266580, China

ARTICLE INFO

Article history:

Received 11 April 2017

Received in revised form

6 June 2017

Accepted 8 June 2017

Available online 10 June 2017

Keywords:

ZnO

Carbon nanofiber

Electrospinning

Li-ion battery

ABSTRACT

For the preparation of higher performance Li-ion batteries, we fabricated a binder-free and self-supported hybrid nanofiber composed of ZnO nanoparticle-decorated core/shell carbon nanofibers (CNFs) by single-nozzle electrospinning of polyvinylpyrrolidone, polyacrylonitrile and zinc acetate dihydrate. After calcination, the hybrid nanofiber can directly serve as binder-free and self-supported anode for Li-ion batteries, which exhibits high capability (723 mA h g^{-1} at 100 mA g^{-1}) and good cycling stability. The CNFs in crisscross structure with good conductivity and strength ensure the fast transportation of electrons and Li ions. In addition, the ca. 2.0 nm amorphous carbon layers on the surface of ZnO nanoparticles can suppress the volume expansion of ZnO in the insertion/extraction of Li ions and improve the cycling stability of ZnO/CNFs, while do not inhibit the transportation of Li ions. These encouraging results suggest a simple and effective method to obtain binder-free and self-supported anode material for Li-ion batteries.

© 2017 Elsevier B.V. All rights reserved.

1. Introduction

Li-ion battery is a widely used energy storage device in modern life and will be used more widely in the future [1]. It is still a challenging but meaningful work to fabricate Li-ion batteries (LIBs) with high performance. The electrode material is known as a key factor to determine the performance of LIBs. With satisfied stability, graphite has been normally used as the commercial anode material of LIBs. However, it has a limited theoretical capacity (372 mA h g^{-1}). Therefore, quantities of attempts have been made to explore or design novel electrode materials to meet the demands on higher capacity and stability. In this field, nanostructured metal oxides (e.g. tin oxide [2–4], zinc oxide [5–7], or iron oxide [8–10]) have got much attention because of their high capacity when used as the anode material in LIBs. Nevertheless, the high volume change in the charge-discharge cycles severely hinders their application. Compared with other metal oxides, ZnO has a great potential to be used as anode material of LIBs due to its readily available and extremely high theoretical capacity (978 mA h g^{-1}) [11]. In order to avoid the severe capacity fade of ZnO anode upon cycling [12],

considerable efforts have been made to strengthen the stability of ZnO while maintain its high capacity [13,14]. In view of the excellent stability of carbon anode in LIBs, an efficient strategy was reinforced by combination the advantages of ZnO and carbon material to prepare ZnO/carbon composites [15,16] with high capacity and excellent stability simultaneously.

The morphology and spatial structure of carbon material in ZnO/carbon composites play important roles on the conductivity of ZnO/carbon material, which should be designed carefully. Kim et al. [17] synthesized a ZnO/activated carbon nanofiber (ACNF) composite by electrospinning and subsequent thermal treatment as a novel anode material for LIBs, which showed good electrical conductivity. The hybrid structure of ACNF offered a short diffusion path for ions and electrons. Wu et al. [15] synthesized a kind of ZnO/mesoporous carbon nanocomposite with polyvinyl alcohol (PVA), zinc nitrate hexahydrate, and ammonium hydroxide, where the carbon matrix derived from PVA acted as the buffer and conducting medium of ZnO/carbon anode. Liu et al. [18] fabricated carbon/ZnO nanorod arrays on nickel substrate by a simple carbonization of pre-adsorbed glucose on ZnO arrays. The cycling stability of ZnO was improved due to the uniform coating of average 6.0 nm carbon shells on ZnO nanorod surface. What's more, the high capacity of ZnO can be maintained as much as possible due to the well-designed structure of ZnO/carbon composite. Sharma et al. [11] fabricated novel anode architecture for

* Corresponding author.

E-mail address: wumb@upc.edu.cn (M. Wu).

¹ These authors contributed equally to this work and should be considered co-first authors.

LIBs by encapsulation of ZnO NPs in the hollow core of reduced graphene oxide (RGO) composite. The interior void spaces combined with the mechanical strength and flexibility of the RGO shell acted as a structural buffer effectively relieving the volumetric stresses generated during charge-discharge cycles. The synergistic effects of the metal oxide, RGO and the core-shell design resulted in a high capacity of 815 mA h g^{-1} at a current density of 50 mA g^{-1} with capacity retention of almost 80% after 100 cycles. Through hydrothermal method and subsequent post-processes, Zhang et al. [19] fabricated a novel structure that ZnO NPs encapsulated in a 3D hierarchical carbon framework (ZnO@CF). The surface carbon coating layer combined with the inside carbon to form a stable 3D carbon framework that encapsulated and anchored the ZnO NPs. The developed ZnO@CF structure not only improved electronic conductivity, but also alleviated the structural strain associated with repeating Li-ion insertion/extraction processes to maintain structural stability. So far, though it is not a new approach to composite ZnO and carbon material as anode of LIBs, there is still a lot of work to do. Further research need to be carried out to improve the capacity and stability of ZnO/carbon material simultaneously.

Herein, we proposed a new strategy to fabricate anode material for LIBs. A nanofiber composed of ZnO NPs decorated CNFs was prepared by single-nozzle electrospinning of polyvinylpyrrolidone (PVP), polyacrylonitrile (PAN) and zinc acetate dihydrate ($\text{Zn}(\text{CH}_3\text{COO})_2 \cdot 2\text{H}_2\text{O}$) following by calcination process. The ZnO/CNFs were directly used as a binder-free anode in LIBs and the reversible capacity and cycling stability were investigated. The CNFs with core/shell structure promoted the homogenous distribution of ZnO NPs. More importantly, ultra-thin carbon layers covered the ZnO surface, fixed the position of ZnO and prevented the expansion of ZnO NPs in the charge-discharge cycles.

2. Experimental

2.1. Composite preparation

In a typical procedure, 1.0 g PAN and 1.0 g PVP were wholly dissolved in 20 mL *N,N*-Dimethylformamide to make solution A. Then 1.0 g $\text{Zn}(\text{CH}_3\text{COO})_2 \cdot 2\text{H}_2\text{O}$ was wholly dissolved in solution A and stirred for 12 h at 45°C to make solution B. For electrospinning process, solution B was transferred into a spinning injector. During the spinning process, the propelling rate of injector was fixed at $25 \mu\text{L s}^{-1}$. The distance between the collecting cylinder (rotary speed 400 r min^{-1}) and the spinning nozzle was 15 cm. The voltage was kept at 22 kV. The obtained electrospun nanofiber was denoted as ZnO/CNF-0.5 precursor. During the calcination process, the ZnO/CNF-0.5 precursor was firstly heated to 240°C in open air under the heating rate of 2°C min^{-1} and kept 3 h for preventing the adhesion of CNF. Then the temperature was raised to 600°C under a heating rate of 3°C min^{-1} in N_2 atmosphere (Zhonghuan SK-1200 furnace, Tianjin, China). The sample was kept at 600°C for 2 h and then cooled to room temperature in N_2 atmosphere. At last, a black mat was obtained and denoted as ZnO/CNF-0.5. With the same procedure, the ZnO/CNF-0, ZnO/CNF-0.25, ZnO/CNF-1.0 and ZnO/CNF-1.5 were prepared. 0, 0.25, 0.5, 1.0 and 1.5 in ZnO/CNF composites represent the mass ration of $\text{Zn}(\text{CH}_3\text{COO})_2 \cdot 2\text{H}_2\text{O}$ to PAN+PVP in solution B. For simplicity, we specified the weight ratio of PVP to PAN as 1:1, while the proportion of $\text{Zn}(\text{CH}_3\text{COO})_2 \cdot 2\text{H}_2\text{O}$ was optimized gradually to obtain the ZnO/CNF composites with the best capacity and stability. For comparison, ZnO/C-0.5 was also prepared with the same procedure of ZnO/CNF-0.5 except PVP was replaced by equal weight of PAN.

2.2. Samples characterization

The functional groups of as-made materials were recorded by Fourier transform infrared spectrometry (FT-IR) (Thermo Nicolet NEXUS 670, USA). The crystal structure of as-made samples was characterized with X-ray diffraction (XRD) (X'Pert PRO MPD, Holland) using Cu K α radiation ($k = 1.518 \text{ \AA}$) in angle of 2 theta from 10 to 75° . Field emission scanning electron microscopy (FE-SEM, S4800, Japan) and transmission electron microscopy (TEM) (JEM-2100UHR, Japan) were used to investigate the morphology of as-obtained samples. The weight loss of the obtained samples was tested by thermogravimetric analysis (TGA) (STA 409 PC Luxx, Germany). The elemental compositions of as-made materials were investigated by XPS analysis (ESCALAB 250, USA).

2.3. Electrochemical measurements

The as-made ZnO/CNFs were directly used as the working electrode. CR2032 coin cells were assembled in an Ar-filled glove box, with lithium foil as counter and reference electrode, polypropylene nanofiber as the separator, and 1 M LiPF_6 in a 1:1 (v/v) mixture of ethylene carbonate and dimethyl carbonate (EC/DMC) as the electrolyte. Cyclic voltammetry (CV) curves were tested at 0.25 mV s^{-1} in the range of 0.005 – 2.8 V by Ametek PARSTAT4000 electrochemistry workstation. The cells were galvanostatically charge-discharged between 0.005 and 2.8 V vs. Li/Li^+ at the current density of 100 mA g^{-1} on a Land CT2001A battery test system.

3. Results and discussion

The FT-IR spectra of ZnO/CNF-0.5 precursor in Fig. S1 exhibits characteristic peaks of PAN ($\text{C}\equiv\text{N}$ stretching vibration, 2240 cm^{-1}), PVP ($\text{C}=\text{O}$ stretching vibration, 1670 cm^{-1}), and zinc acetate ($\text{O}-\text{C}=\text{O}$ stretching vibration, 1600 cm^{-1}). After pre-oxidization of ZnO/CNF-0.5 precursor, the stretching vibration peak of $\text{C}\equiv\text{N}$ at 2240 cm^{-1} almost disappears and a new broad peak at 1650 cm^{-1} appears due to the cyclization reaction of $\text{C}\equiv\text{N}$ in PAN to $\text{N}-\text{C}=\text{N}$ at 240°C . After carbonation, the peaks at 2920 cm^{-1} (stretching vibration of $\text{C}-\text{H}$) and 1420 cm^{-1} (bending vibration of $\text{C}-\text{H}$) vanish, which indicate the carbonation reactions take place at 600°C .

To further investigate the chemical compositions of ZnO/CNF-0.5, the XPS analysis was carried out, as revealed in Fig. 1. The characteristic peaks of C1s, N1s, O1s and Zn2p all exist in Fig. 1(a), which indicate that the ZnO/CNF composites are mainly composed by C, N, O and Zn elements. Fig. 1(b) has two main nitrogen species, pyridinic N (398.2 eV) and pyrrolic N (399.9 eV) [20]. The cavity and electron defects of pyridinic N atoms promote the transfer rates of electrons and Li ions, which further improve the electrochemical performance of ZnO/CNFs [21,22].

The morphology of ZnO/CNF-0.5 was characterized by SEM, as revealed in Fig. 2. The SEM image in Fig. 2(a) shows one-dimensional polymer nanofiber of ZnO/CNF-0.5 precursor with smooth surface and uniform diameter of 220 nm (calculated). After calcination, ZnO/CNFs keep a similar one-dimensional nanofiber structure, while numerous hemispherical ZnO NPs uniformly deposits on the surface, as revealed in Fig. 2(b).

XRD patterns of ZnO/CNFs are shown in Fig. S2. For ZnO/CNF-0 nanofiber, a broad diffraction peak assigned to the characteristic (002) reflection of carbon can be found at 24° , suggesting the existence of large amount of amorphous carbon. The high-resolution XPS spectrum and the fitting curves of the C1s further verify the existence of amorphous carbon. As shown in Fig. 1(c), the C1s spectrum can be deconvoluted into four peaks, of which the highest fitting peak at 284.7 eV represents $\text{C}-\text{C}$ bond. The other weaker fitting peaks at 285.6 , 286.8 , and 288.9 eV are assigned to $\text{C}-\text{N}$, $\text{C}=\text{C}$

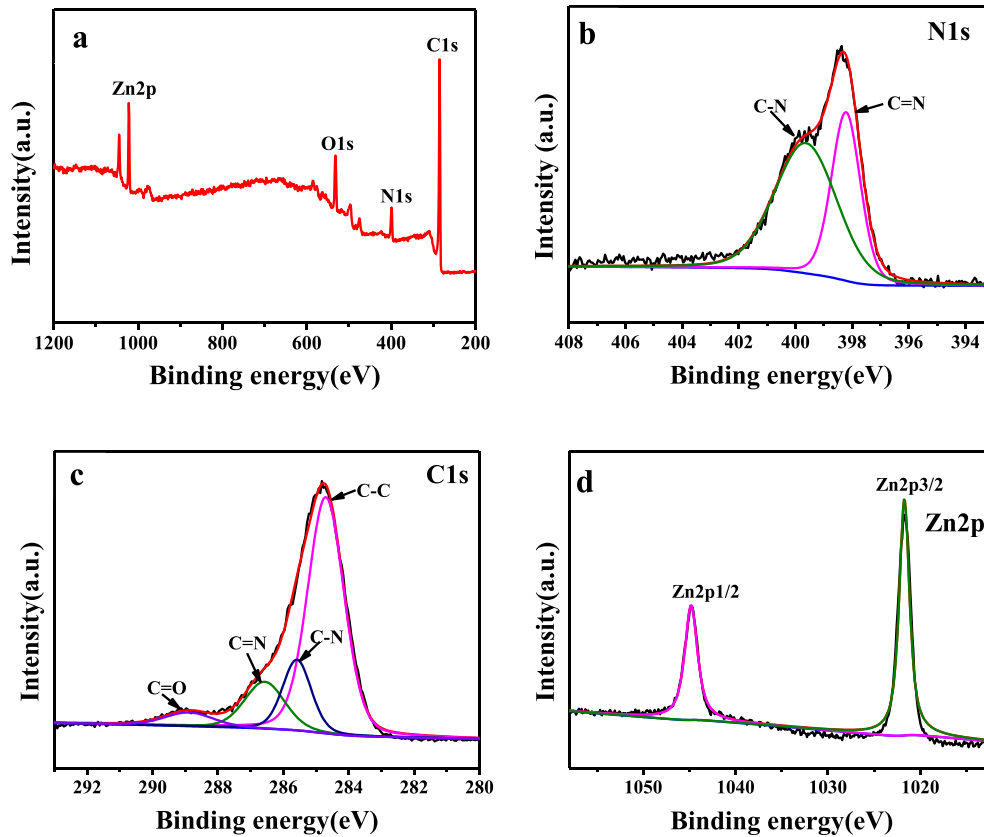


Fig. 1. (a) XPS survey scans of ZnO/CNF-0.5; (b) High-resolution XPS N1s spectrum; (c) High-resolution XPS C1s spectrum; (d) High-resolution XPS Zn2p spectrum.

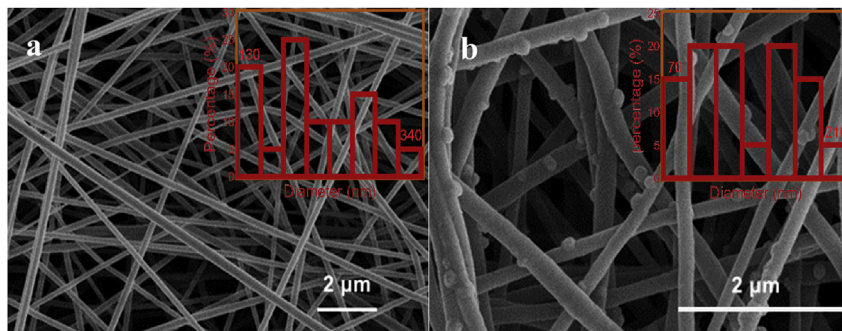


Fig. 2. SEM images: (a) ZnO/CNF-0.5 precursor and (b) ZnO/CNF-0.5.

N and C=O bonds, respectively. The characteristic peaks of 31.8° , 34.4° , 36.3° and 56.6° are indexed to the (100), (002), (101) and (110) crystal planes of the hexagonal ZnO crystalline structure [6,15], which is consistent with the standard ZnO crystal structure as revealed in the bottom of Fig. S2. The detailed valence state of Zn element in the composite can be further confirmed by the XPS spectrum in Fig. 1(d). According to the Scherrer formula [23], the crystal size is inversely proportional to its half-height width of diffraction peak in the XRD spectra. With the increasing content of ZnO, the diffraction peak of ZnO in ZnO/CNFs are significantly enhanced, which indicate that the crystalline degree of ZnO is gradually decreased in the following order, ZnO/CNF-1.0 > ZnO/CNF-0.5 > ZnO/CNF-0.25. It is clearly seen that the crystalline size of ZnO in ZnO/CNFs can be adjusted by the content of $\text{Zn}(\text{CH}_3\text{COO})_2 \cdot 2\text{H}_2\text{O}$ in the precursors.

Furthermore, the details of ZnO status in ZnO/CNF-0.5 nanofiber

were investigated by TEM. As shown in Fig. 3(a), the preoxidized ZnO/CNF-0.5 has a diameter of 160 nm with a core/shell structure. In consistency with the result of He et al. [24], the core of ZnO/CNF-0.5 is derived from the carbonization of PAN while the shell is derived from the carbonization of PVP, the thickness of the shell is about 24 nm, and the black particles are ZnO NPs. As is more affinity with PVP, ZnO gradually move to the shell layers during the heat treatment and transform to hemispherical ZnO NPs along with the carbonization of PVP. Fig. 3(c) displays the distribution of ZnO NPs on the surface of ZnO/C-0.5, which is fine and uniform (less than 100 nm), and obviously different with that of ZnO/CNF-0.5, confirming that added PVP can promote the formation of hemispherical ZnO NPs on the surface of CNFs. Consequently, the ca. 2.0 nm amorphous carbon layers (Fig. 3(d)) outside of ZnO NPs in ZnO/CNF-0.5 are from the carbonization of PVP.

This hybrid structure can effectively inhibit the volume

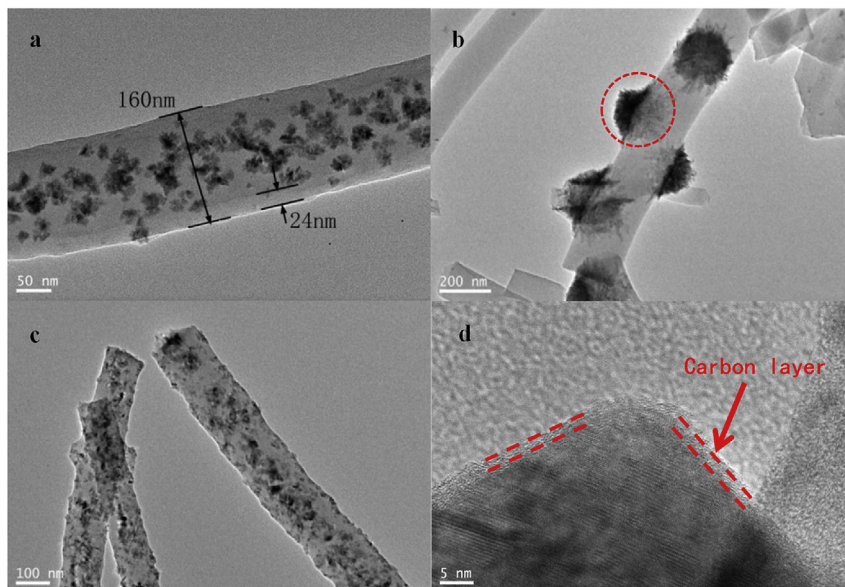


Fig. 3. TEM images: (a) pre-oxidized ZnO/CNF-0.5; (b) ZnO/CNF-0.5; (c) ZnO/C-0.5; (d) HR-TEM image of ZnO/CNF-0.5.

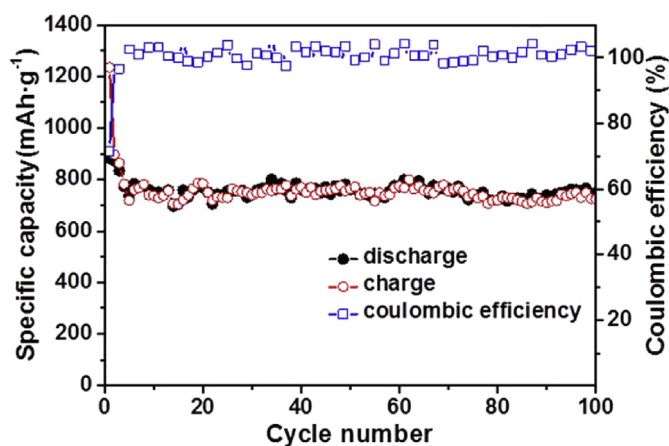


Fig. 4. Cyclic performance of ZnO/CNF-0.5 at the current density of 100 mA g^{-1} .

expansion of ZnO NPs in the charge-discharge cycles, while the ultrathin carbon layers do not block the insertion/extraction of Li ions. The content of ZnO in ZnO/CNF-0.5 tested by TGA analysis under air atmosphere is shown in Fig. S3. The main weight loss of ZnO/CNF-0.5 takes place in the range of $400\text{--}600^\circ\text{C}$ and no weight loss after 600°C , this big weight loss corresponds to the combustion of carbon. Accordingly, the weight ratio of ZnO in ZnO/CNF-0.5 nanofiber is calculated to 28.7%.

The as-prepared ZnO/CNFs were directly used as the anode of LIBs, and their electrochemical performance was investigated. Firstly, the redox reaction of the ZnO/CNFs was evaluated by cyclic voltammetry under the scan rate of 0.25 mV s^{-1} for 5 cycles (Fig. S4). For ZnO/CNF-0.5 anode, a reduction peak between 0.8 and 0.3 V is only founded in the first circle, which is attributed to the formation of SEI film during Li-ion inserting reaction [6]. It is known that the SEI formed is irreversible, thus the platform about 0.7 V is not found in following circles. Another reduction peak appears between 0.3 and 0 V is attributed to the alloying reaction of zinc and lithium. The CV curves are substantially coincident in the following cycles, indicating that the ZnO/CNF-0.5 nanofiber has a good reversibility in the charge-discharge cycles.

Furthermore, the charge-discharge performance of ZnO/CNF-0.5 anode was tested at current density of 100 mA g^{-1} , as revealed in Fig. S5 and Fig. 4. It can be seen in Fig. S5 that the first discharging capacity of ZnO/CNF-0.5 is 1233 mA h g^{-1} while the first charging capacity is 882 mA h g^{-1} , and a relative high initial coulombic efficiency of 71.5% can be obtained. As shown in Fig. 4, though there is an apparent decline of capacity in the first charge-discharge cycle, a high reversible capacity of 723 mA h g^{-1} after 100 cycles can be kept, with nearly 100% coulombic efficiency maintained, which indicate that ZnO/CNF-0.5 anode has good cycling stability. After 100 charge-discharge cycles, the reversible capacities of ZnO/CNF-0.25, ZnO/CNF-0.5, ZnO/CNF-1.0, ZnO/CNF-1.5, ZnO/CNF-0 and ZnO/C-0.5 at 100 mA g^{-1} are listed in Table S1. Compared with pure CNFs (ZnO/CNF-0), all ZnO/CNFs except ZnO/CNF-1.5 show higher reversible capacity while ZnO/CNF-0.5 has the highest capacity, which indicate ZnO NPs with appropriate content and morphology help to improve the reversible capacity of the CNFs [25]. Compared with ZnO/C-0.5, ZnO/CNF-0.5 has a better cycling stability mainly

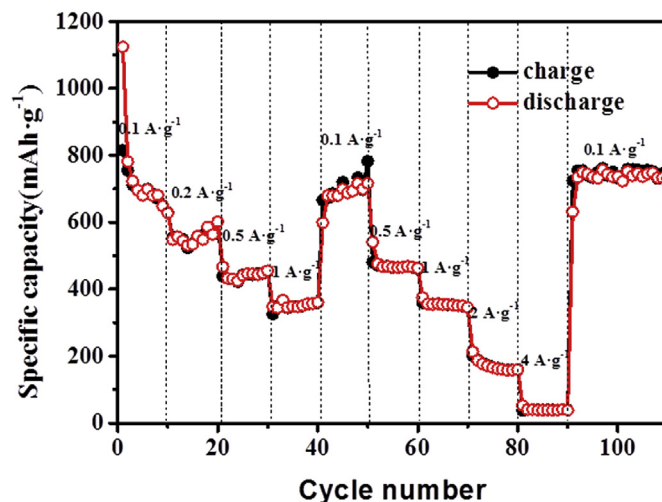


Fig. 5. Rate performance of ZnO/CNF-0.5.

because of the ultra-thin carbon layer coated on ZnO NPs (Fig. 3(d)). The carbon layers formed by the carbonization of PVP can fix the position and inhibit the volume expansion of ZnO NPs during the charge-discharge cycles. All above factors make ZnO/CNF-0.5 as prepared has relatively high capacity under 100 mA g⁻¹ compared with the literature data listed in Table S1.

The rate performance of ZnO/CNF-0.5 was also tested, as shown in Fig. 5. Under different current densities, as in the order of 0.1, 0.2, 0.5, 1.0, 0.1, 0.5, 1.0, 2.0, 4.0, 100 mA g⁻¹, the reversible capacities of LIBs are listed in Table S2. Even after a serious of charge-discharge under different current densities, the reversible capacity of LIBs can be well recovered when the current density goes back to 100 mA g⁻¹. SEM image of the used ZnO/CNF-0.5 anode is given in Fig. S6. The network structure of CNFs can be well kept even after long charge-discharge cycles, which indicate that the steady nanostructure of ZnO/CNF ensures its high cycling stability.

4. Conclusion

In summary, ZnO/CNFs were successfully prepared by single-nozzle electrospinning and subsequently calcination process. The obtained CNFs had a core/shell structure derived from the carbonation of PAN and PVP, respectively. The hemispherical ZnO NPs covered by ca. 2.0 nm amorphous carbon layers deposited uniformly on the surface of CNFs. Directly served as a binder-free and self-supported anode of LIBs, the hierarchical structure of ZnO/CNF anode facilitates the diffusion of Li ions and electrolyte. The stable conductive network formed by the crisscross CNFs ensures high speed transmission of electrons. The unique coating structures of ZnO NPs covered by amorphous carbon layers fix ZnO and inhibit its volume expansion during the charge-discharge cycles. Therefore, LIBs assembled by binder-free ZnO/CNFs anode exhibit improved electrochemical performance, including high specific capacity, excellent rate capability, and enhanced cycling stability. This work provides a simple and effective method to obtain binder-free and self-supported anode material for Li ion batteries.

Acknowledgements

This work was supported by the National Natural Science Foundation of China (Nos. 51372277, 51572296, U1662113); the Fundamental Research Fund for the Central Universities (No. 15CX08005A, 14CX02127A).

Appendix A. Supplementary data

Supplementary data related to this article can be found at <http://dx.doi.org/10.1016/j.jallcom.2017.06.099>.

References

- [1] K. Yamaguchi, Y. Domi, H. Usui, M. Shimizu, K. Matsumoto, T. Nokami, T. Itoh, H. Sakaguchi, *J. Power Sources* 338 (2017) 103–107.
- [2] X.Y. Li, Y.Q. Qu, *Cryst. Growth. Des.* 16 (2016) 34–41.
- [3] N. Mohri, B. Oschmann, N. Laszczynski, F. Mueller, J. von Zamory, M.N. Tahir, S. Passerini, R. Zentel, W. Tremel, *J. Mater. Chem. A* 4 (2016) 612–619.
- [4] Y.H. Sun, P.P. Dong, S. Liu, J.M. Nan, *Mater. Res. Bull.* 74 (2016) 299–310.
- [5] Y. Liu, Y. Li, M. Zhong, Y.M. Hu, P.F. Hua, M.Y. Zhu, W.X. Li, Y.B. Li, *Mater. Lett.* 171 (2016) 244–247.
- [6] E. Quartarone, V. Dall'Asta, A. Resmini, C. Tealdi, I.G. Tredici, U.A. Tamburini, P. Mustarelli, *J. Power Sources* 320 (2016) 314–321.
- [7] B.N. Joshi, S. An, H.S. Jo, K.Y. Song, H.G. Park, S. Hwang, S.S. Al-Deyab, W.Y. Yoon, S.S. Yoon, *ACS Appl. Mater. Inter.* 8 (2016) 9446–9453.
- [8] X. Cai, H.B. Lin, X.W. Zheng, X.Q. Chen, P. Xia, X.Y. Luo, X.X. Zhong, X.P. Li, W.S. Li, *Electrochim. Acta* 191 (2016) 767–775.
- [9] Y. Luo, L.H. Liu, W.C. Qiao, F. Liu, Y.S. Zhang, W.F. Tan, G.H. Qiu, *Mater. Chem. Phys.* 170 (2016) 239–245.
- [10] Y.S. Wu, L. Zhan, K.T. Huang, H.J. Wang, H. Yu, S.Q. Wang, F. Peng, C.Y. Lai, *J. Alloy Compd.* 684 (2016) 47–54.
- [11] B.M. Shilpa, S.B. Basavaraja, A. Majumder, J. Sharma, *Mater. Chem. A* 3 (2015) 5344–5351.
- [12] G.Z. Yang, H.W. Song, H. Cui, Y.C. Liu, C.X. Wang, *Nano Energy* 2 (2013) 579–585.
- [13] W. Yin, Y. Shen, F. Zou, X.L. Hu, B. Chi, Y.H. Huang, *ACS Appl. Mater. Inter.* 7 (2015) 4947–4954.
- [14] G.H. Zhang, S.C. Hou, H. Zhang, W. Zeng, F.L. Yan, C.C. Li, H.G. Duan, *Adv. Mater.* 27 (2015) 2400–2405.
- [15] P. Li, Y. Liu, J.Y. Liu, Z.T. Li, G.L. Wu, M.B. Wu, *Chem. Eng. J.* 271 (2015) 173–179.
- [16] C.L. Xiao, S.C. Zhang, S.B. Wang, Y.L. Xing, R.X. Lin, X. Wei, W.X. Wang, *Electrochim. Acta* 189 (2016) 245–251.
- [17] S.Y. Kim, B.H. Kim, *Synth. Met.* 210 (2015) 386–391.
- [18] J.P. Liu, Y.Y. Li, R.M. Ding, J. Jiang, Y.Y. Hu, X.X. Ji, Q.B. Chi, Z.H. Zhu, X.T. Huang, *J. Phys. Chem. C* 113 (2009) 5336–5339.
- [19] C.L. Xiao, S.C. Zhang, S.B. Wang, Y.L. Xing, R.X. Lin, X. Wei, W.X. Wang, *Electrochim. Acta* 189 (2016) 245–251.
- [20] B. Kumar, M. Asadi, D. Pisasale, S. Sinha-Ray, B.A. Rosen, R. Haasch, J. Abiade, A.L. Yarin, A. Salehi-Khojin, *Nat. Commun.* 4 (2013) 2389.
- [21] J. Liang, C.H. Xiao, X. Chen, R.X. Gao, S.J. Ding, *Nanotechnology* 27 (2016) 8.
- [22] L.C. Yang, W. Sun, Z.W. Zhong, J.W. Liu, Q.S. Gao, R.Z. Hu, M. Zhu, *J. Power Sources* 306 (2016) 78–84.
- [23] A.W. Burton, K. Ong, T. Rea, I.Y. Chan, *Micropor. Mesopor. Mat.* 117 (2009) 75–90.
- [24] H.R. Xue, X.W. Mu, J. Tang, X.L. Fan, H. Gong, T. Wang, J.P. He, Y. Yamauchi, *J. Mater. Chem. A* 4 (2016) 9106–9112.
- [25] T. Jammongkan, R. Shirota, S.K. Sukumaran, M. Sugimoto, K. Koyama, *Polym. Eng. Sci.* 54 (2014) 1969–1975.